
CARSO: Counter-Adversarial Recall of Synthetic Observations

Emanuele Ballarin 

AILAB
University of Trieste
Trieste, Italy
emanuele@ballarin.cc

Alessio Ansuini* 

Data Engineering Laboratory
AREA Science Park
Trieste, Italy
alessio.ansuini@areasciencepark.it

Luca Bortolussi* 

AILAB
University of Trieste
Trieste, Italy
lbortolussi@units.it

Abstract

In this paper, we propose a novel adversarial defence mechanism for image classification – CARSO – inspired by cues from cognitive neuroscience. The method is synergistically complementary to adversarial training and relies on knowledge of the *internal representation* of the attacked classifier. Exploiting a generative model for adversarial purification, conditioned on such representation, it samples reconstructions of inputs to be finally classified.

Experimental evaluation by a well-established benchmark of varied, strong adaptive attacks, across diverse image datasets and classifier architectures, shows that CARSO is able to defend the classifier significantly better than *state-of-the-art* adversarial training alone – with a tolerable *clean* accuracy toll. Furthermore, the defensive architecture succeeds in effectively shielding itself from unforeseen threats, and *end-to-end* attacks adapted to fool stochastic defences.

1 Introduction

Vulnerability to adversarial attacks [6, 61] – *i.e.* the presence of specific inputs, usually crafted on purpose, able to catastrophically alter the behaviour of high-dimensional models [7] – constitutes a major hurdle towards ensuring compliance of deep learning systems with the behaviour expected by modellers and users, and their adoption in safety-critical scenarios or tightly-regulated environments. This is particularly true for adversarially-*perturbed* inputs, where a norm-constrained perturbation – often hardly detectable by human inspection [51, 4] – is added to an otherwise legitimate input, with the intention of eliciting a potentially malicious anomalous response [36].

Given the pervasiveness of the issue [29], and the serious concerns raised about safety and reliability of data-learned models in the lack of appropriate mitigation [5], adversarial attacks have been extensively studied. Yet, that of obtaining generally-robust machine learning (*ML*) systems remains a longstanding issue, and a major open challenge.

Research in the field has been animated by two opposing (yet complementary) efforts. On the one hand, the study of *failure modes* in existing models and defences, with the goal of understanding their origin and developing stronger attacks with varying degrees of knowledge and control over the

*Joint supervision.

target system [61, 19, 47, 65]. On the other hand, the construction of increasingly capable defence mechanisms. Though alternatives have been explored [11, 64, 9, 74], most part of the latter is based on adequately leveraging *adversarial training* [19, 43, 63, 52, 21, 32, 58, 69], *i.e.* training a *ML* model on a dataset composed of (or enriched with) adversarially-perturbed inputs associated with their correct, *pre-perturbation* labels. And indeed, adversarial training has been the only technique so far able to consistently provide an acceptable level of defence [22], while still incrementally improving upon itself, up to current *state-of-the-art* [52, 21].

Another defensive approach is that of *adversarial purification* [57, 73], where a generative model is used – akin to denoising – to recover a perturbation-free version of the input before classification occurs. Nonetheless, such attempts have generally fallen short of expectations due to inherent limitations of the generative models used, or due to decreases in robust accuracy¹ when attacked *end-to-end* [23] – resulting in subpar robustness when the defensive structure is known to the adversary [65]. More recently, the rise of diffusion-based generative models [26] enabled more successful results [48] – though still at the cost of relatively lengthy training and significantly longer inference times.

In parallel to such endeavours, considerable efforts have also been put towards the development of standardised evaluation protocols for newly-proposed adversarial defence strategies [10, 13, 14] – whose impact may often be masked or overstated [27] due to methodological fragmentation [67] or overspecialisation of defences [54].

In this work, we draw inspiration from neurocognitive processes underlying *cued recall* and *recognition* [66, 18, 44] to devise a novel adversarial purification mechanism for supervised image classifiers. The approach proposed – relying on a *conditional* [60, 72] *variational autoencoder* [34, 53] as the generative model of choice, and on an adversarially-pretrained classifier – tightly couples the *purification* phase with the subsequent classification, by conditioning the process of input denoising on the ordered tensor² of activations registered at neuron level in the classifier. At inference, a sample of reconstructions is classified, and labels finally assigned by majority vote.

The architecture just outlined – retaining synergistic operation with well-established adversarial training techniques – is further complemented with a *bag of* theoretically-justified *tricks*: chiefly the use of a fixed *batchwise* fraction of adversarially-perturbed inputs during training, and the learnable pre-encoding, before *autoencoding*, of *internal representations* and images.

Empirical testing³ of the defensive capabilities of the method is also provided. Various classifier architectures (*FCNs*, *CNNs* [38], *RESNETs* [24]), adversarially-trained according to different protocols – including *state-of-the-art* pretrained models [52] – on the *MNIST* [39], *FASHIONMNIST* [71] and *CIFAR-10* [35] image datasets, are shown to significantly benefit from the addition of *CARSO* *w.r.t.* their robust accuracy, at tolerable *clean accuracy*⁴ cost. This remains true in the case of attacks deliberately outside the threat model adopted during training, of greater strength, or specifically devised to assess the general robustness of defensive strategies against unforeseen attacks – even when adapted to fool stochastic defences, such as *CARSO*.

Summarising, the paper makes the following contributions:

- A novel adversarial purification mechanism: in essence, a denoising variational autoencoder conditioned on the *internal representation* of an adversarially-pretrained classifier;
- A theoretically-justified *bag of tricks* to make possible, and further ease, the training of such architecture;
- Experimental assessment of the method proposed, including against standardised benchmark adversarial attacks – showing higher robust accuracy *w.r.t.* to (even *state-of-the-art*) adversarial training, and defying direct, *end-to-end* attacks.

The rest of the manuscript is structured as follows. In section 2 we provide an overview of contributions in the fields of *adversarial training* and *purification-based* defences – with focus on image

¹ The *test set accuracy* of the frozen-weights trained classifier – computed on a dataset entirely composed of adversarially-perturbed examples, generated against the classifier itself.

² Which we call *internal representation*.

³ Implementation of the method and code for the experiments (based on *PyTorch* [49], *AdverTorch* [16], *TorchAttacks* [33], and *ebtorch*) can be found at: <https://github.com/emaballarín/CARSO>.

⁴ The *test set accuracy* of the trained classifier – computed on a dataset composed of unperturbed data.

classification. In section 3, a deeper analysis is given of two integral parts to our contribution: PGD adversarial training, and (conditional) variational autoencoders. Section 4 is dedicated to the intuition behind CARSO, its architectural description, and the *tricks* used during its training. Section 5 contains details about experimental setup, results, and comments. Section 6 concludes the paper.

2 Related Work

Adversarial training as a defence The idea of training a model on adversarially-generated examples as a way to make it more robust can be traced back to the very beginning of research in the area. The seminal [61] proposes to perform training on a mixture of *clean* and adversarial data, generated beforehand.

The introduction of FGSM in [19] enables the efficient generation of adversarial examples during training – with a single normalised gradient step. Incremental improvements include R+FGSM [64] – that adds a randomisation step to FGSM – and BIM [36], where multiple smaller steps are taken in the direction of the local gradient.

A significant leap forward came with PGD [43] – discussed detailedly in section 3. The remarkable effectiveness of such method [22] makes it still the standard *de facto* for the synthesis of adversarial training examples. Further incremental improvements have also been developed, some focused on robustness assessment (*e.g.* adaptive-stepsize variants, as in [13]).

Concerns about *robust overfitting* [54] spurred further research into strategies to reduce overadaptation of adversarially-trained models. Surprisingly, it appeared that beyond-trivial data augmentation schemes – very effective in promoting generalisation in the *clean* regime [24] – were instead scarcely useful as a complement to adversarial training [54, 22]. Very recent work [52] counters such claim, showing that the joint effect of training data augmentation and weight averaging [31] does indeed improve model robustness.

Purification as a defence Among the first attempts of *purification-based* adversarial defence, [23] investigates the use of denoising autoencoders [68] to recover examples free from adversarial perturbations. Despite its effectiveness in the denoising task, the method may indeed increase the vulnerability of the network when attacks are generated against it as a whole. The improvement proposed – *Deep Contractive Networks* – adds a smoothness penalty to the reconstruction loss, mitigating such downside. Similar in spirit, [41] tackles the issue by computing reconstruction loss between the last-layers representations of the (frozen-weights) attacked classifier, receiving respectively as input the *clean* and the tentatively *denoised* example.

In [56], *Generative Adversarial Networks* [20] (GANs) learned on *clean* data are used at inference time to find a synthetic plausible example belonging to the unperturbed data manifold, that is the closest to perturbed input. Despite positive results, the delicate training process of GANs and the existence of known failure modes [76] affects the method. More recently, a similar approach [25] employing *energy-based models* [40] suffered from poor sample quality.

Purification approaches based on (conditional) variational autoencoders include [28] and [57].

Finally, already-mentioned techniques relying on *score-* [73] and *diffusion-* based [48] models have also been proposed, with surprisingly favourable and general results – often balanced in practice by longer training and inference times.

To the best of our knowledge and bibliographic research, our contribution is the first that explicitly blends the paradigms of *adversarial training* and *purification* beyond the possibility of simple juxtaposition of the two.

3 Preliminaries

PGD adversarial training The task of finding model parameters θ^* robust to adversarial perturbations is framed in [43] as a *min-max* optimisation problem seeking to minimise *adversarial risk*, *i.e.*:

$$\theta^* \approx \hat{\theta}^* := \arg \min_{\theta} \mathbb{E}_{(\mathbf{x}, y) \sim \mathcal{D}} \left[\max_{\delta \in \mathbb{S}} \mathcal{L}(f(\mathbf{x} + \delta; \theta), y) \right]$$

where \mathcal{D} is the distribution over examples \mathbf{x} and labels y , $f(\cdot; \theta)$ is a model with learnable parameters θ , \mathcal{L} is a suitable loss function, and \mathbb{S} is the set of allowed perturbations. In the case of ℓ_p norm-bound perturbations of maximum magnitude ϵ , we can specify $\mathbb{S} := \{\delta \mid \|\delta\|_p \leq \epsilon\}$.

The inner optimisation problem is solved in [43] by *Projected Gradient Descent* (PGD), an iterative algorithm whose goal is the synthesis of adversarial perturbation $\hat{\delta} = \delta^{(K)}$ after K gradient ascent steps defined as:

$$\delta^{(k+1)} \leftarrow \mathfrak{P}_{\mathbb{S}} \left(\delta^{(k)} + \alpha \text{sign} \left(\nabla_{\delta^{(k)}} \mathcal{L}_{ce}(f(\mathbf{x} + \delta^{(k)}; \theta), y) \right) \right)$$

where $\delta^{(0)}$ is randomly sampled within \mathbb{S} , α is a hyperparameter (*step size*), \mathcal{L}_{ce} is the cross-entropy function, and $\mathfrak{P}_{\mathbb{A}}$ is the Euclidean projection operator onto set \mathbb{A} , *i.e.* $\mathfrak{P}_{\mathbb{A}}(\mathbf{a}) := \arg \min_{\mathbf{a}' \in \mathbb{A}} \|\mathbf{a} - \mathbf{a}'\|_2$. The outer optimisation is carried out by simply training $f(\cdot; \theta)$ on the examples found by PGD against current model parameters – and their pre-perturbation labels.

In this manuscript, we will use the shorthand notation ϵ_p to denote ℓ_p norm-bound perturbations of maximum magnitude ϵ ; we will refer to k -steps PGD as PGD^K .

(Conditional) Variational Autoencoders Variational autoencoders (VAEs) [34, 53] allow the learning from data of approximate generative latent-variable models of the form $p(\mathbf{x}, \mathbf{z}) = p(\mathbf{x} \mid \mathbf{z})p(\mathbf{z})$, whose likelihood and approximate posterior are parameterised by deep artificial neural networks (ANNs). The problem is cast as maximisation of a variational lower bound.

In practice, optimisation is performed iteratively – on a loss determined by a mixture of reconstruction loss and empirical *KL* divergence *w.r.t.* the prior, computed on minibatches of data. Further details on the functioning of (conditional) VAEs are given in Appendix A.

Conditional Variational Autoencoders [60, 72] extend VAEs by concatenating a *conditioning vector* \mathbf{c} – expressing specific characteristics of each example – to \mathbf{z} during training. This allows the learning of a decoder model capable of conditional data generation.

4 Development and structure of CARSO

The core ideas informing the design of our method are driven more by *first-principles* and *analogical* reasoning rather than arising from direct formal requirements. This section is dedicated to the discussion of such ideas, the specification of the architectural details of CARSO, and to practical enhancements to its training process.

4.1 Architectural overview and principle of operation

From a purely architectural viewpoint, CARSO is composed of an ANN-based classification model and a conditional VAE, operating in synergy. The only requirement of the former is that of having been adversarially trained to solve the classification task of interest – thus allowing the reuse of pre-trained models and retaining the contribution to overall robustness from established adversarial training techniques.

The key element of novelty lies in the intertwined operation of *model* and VAE – aimed at learning a distribution of purified examples (to be generated from each potentially-perturbed input), and to classify samples harvested from it – without increasing the overall vulnerability in the process.

Training During training, examples are corrupted with adversarial perturbations against the pre-trained model. Those are fed to the latter, and the tensor of its activations across all layers (in arbitrary, but fixed, order) extracted. The conditional VAE is then trained on denoised input reconstruction, conditioned on their corresponding *internal representation*.

Upon completion of the training process, the encoder network may be discarded.

Inference The example requiring classification is fed to the pre-trained model. Its corresponding internal representation is extracted and used to condition the generative process described by the decoder of the VAE – whose latent variables are sampled from their original priors. Each element in the resulting set of denoised examples is classified by the pre-trained model, and individually predicted classes are aggregated (*e.g.* by simply taking the mode). Result of the aggregation is the robust prediction of the input class.

Remarkably, the only link between the initial potentially-perturbed input and the resulting purified reconstructions (and thus, predicted class) is through the *internal representation* of the classifier.

4.2 A first-principles justification

If we consider a trained ANN classifier, subject to a successful adversarial attack by means of a slightly perturbed example, we observe that – both in terms of ℓ_p magnitude and human perception – a small variation on the input side of the network is amplified to a significant amount on the output side, thanks to the layerwise processing by the model. Given the deterministic nature of such processing at inference time, we can conclude that also the *trace* obtained by sequentially collecting the activation values produced within the layers of the network along the forward pass will be different between a *perturbed* example and its *clean* counterpart.

Naively, one could imagine to learn to perform adversarial input detection by analysing such *internal representation*. The issue introduced by this approach, though, is threefold: (a) the resulting architecture would become in turn adversarially-attackable, without reasonable guarantees of increased robustness; (b) even in case of correct labelling of an adversarially-perturbed input, no direct recovery of the correct pre-perturbation label is made possible; (c) detection of adversarial examples is inherently hard, almost as robust classification is [62].

The issues raised in (b) and (c) are addressed by using the same *internal representation* to inform an adversarial purification process instead, leaving final classification to a proper classifier.

As far as claim (a) is concerned – if the model used for *internal representation* extraction is the same as that performing classification of the reconstructions – we conjecture that the architecture has positive effects on robustness, by decreasing *end-to-end* attackability. Indeed, if one considers the total gradient arising at the level of individual neurons in the classifier – *e.g.* when a gradient-based adversarial attack is performed against the whole architecture – it is the result of those neurons playing two roles at once: within the input/output mapping determining the classification of reconstructions, and as a feature in the *internal representation* extraction process. Since the individual directions of those gradients are *a priori* not aligned, it is likely that – at least in expectation – partial gradient interference occurs, preventing perturbations towards directions of maximum vulnerability of the unshielded classifier. Such claim is further corroborated by experimental results reported in section 5.

4.3 Example and internal representation pre-encoding

Given the high variability of datasets and classifier architectures across instances of robust classification – one potential limitation of the approach described so far comes from the heterogeneity in relative size and structure between data \mathbf{x} to be modelled and their corresponding conditioning set \mathbf{c} . Indeed, the training of a conditional VAE requires [60] concatenation of the two, and further concatenation of the latter with a sample of latent variables $\mathbf{z} \sim q_{\theta_E}(\mathbf{z} | \mathbf{x}; \theta_E)$.

As a motivating example, in robust classification of *e.g.* MNIST [39] images (786 scalars each) by means of a very small *fully-connected network* (≈ 300 neurons total), the $|\mathbf{c}|/|\mathbf{x}|$ ratio is wildly different *w.r.t.* *e.g.* IMAGENET-like [15] data ($\approx 5 \times 10^5$ scalars per image) classified by a deep RESNET ($\approx k \times 10^6$ neurons).

Additionally, the *a priori* lack of spatial structure in \mathbf{c} strongly limits the use of *convolutional neural networks* (CNNs) within the encoder, whereas the use of *fully-connected networks* (FCNs) on images is deemed unsatisfactory – given the hardness of learning locally-convolutional structures from data [30].

Mitigating both issues, we propose to insert in the architecture two additional *auxiliary* encoders – again parameterised by ANNs – to be learned jointly with the VAE during training on the purification task: one relative to data $\mathcal{D}(\cdot; \theta_{\mathcal{D}})$ and one to the *context* $\mathcal{C}(\cdot; \theta_{\mathcal{C}})$.

The resulting *encoded* examples $x' := \mathcal{D}(x; \theta_{\mathcal{D}})$ and context $c' := \mathcal{C}(c; \theta_{\mathcal{C}})$ may be used in place of x and c respectively, within the VAE. This allows to effectively decouple data- and context-specific processing before *autoencoding* occurs: in the design of \mathcal{D} and \mathcal{C} , the $|c|/|x|$ balance is ensured by tuning output sizes; structural heterogeneity is addressed by choosing the inductive biases [46] deemed the most suitable to respective inputs.

In order to sample from the generative model at inference time, \mathcal{C} must be preserved after training, and used to encode the *internal representations*.

4.4 Adversarially-balanced batches

Another impacting issue is the high instability in training the purifier. Such effect is caused by the composition, and the specific manner and order of presentation, of the set of adversarial examples (and associated *internal representation*) shown to the VAE during training.

Conjecturing that most of the observed decrease in robustness depends on the inability to recover pre-perturbation examples from adversarially-attacked images generated differently from those in the training set, the composition of perturbations is adapted to mitigate the issue. Justificatory footing to such consideration is illustrated in Appendix B.

By calling ϵ the maximum ℓ_p norm bound of the threat model against which the classifier was hardened, the purifier is trained against a mixture of *clean* and *perturbed* examples – the latter split evenly among FGSM $_{\epsilon/2}$, PGD $_{\epsilon/2}$, FGSM $_{\epsilon}$, and PGD $_{\epsilon}$.

To further mitigate metastable behaviour arising from sequential presentation to the VAE of batch-homogeneous (un)perturbed examples along weight-update steps, care is put towards the generation of batches equally representative of the different types and strengths of attacks, while relying on dataset randomisation to benefit from regularisation due to stochastic approximation [55, 8]. Within an epoch of training, of each of the *clean* batches resulting from the shuffled dataset, a fixed fraction is kept unprocessed – whereas the remaining portion evenly perturbed across the attacks listed above.

4.5 Instance-specific tuning

The method just described provides a rather general and flexible framework for the *add-on* shielding of adversarially-trained classifiers. Further tuning of the VAE and its usage protocol are possible – and mostly dependent on the specific data of interest.

In our investigation, we focused on image data. As a consequence, *e.g.*, we restricted the reconstruction task to the image alone (instead of also including the conditioning tensor, as common practice with *class-conditional VAEs*) and designed the decoder of the purifier as a Deep Generative Deconvolutional Network (DGDN) [50].

Finally, as a way to ease scalability – proportional to the number of neurons in the classifier – of the purifier input, a carefully-chosen subset of layers is used instead of the whole *internal representation*, when needed. Such *trick*, used extensively in experiments, does not significantly compromise the effectiveness of CARSO while providing tangible computational benefits.

Details related to architectural choices and hyperparameters are described in section 5 and in Appendix C. A visual schematic of the overall architecture of CARSO is provided in Appendix E.

5 Experimental assessment

Experimental evaluation of CARSO in improving upon robust accuracy of adversarially-pretrained image classifiers is carried out within different scenarios. The *white-box* setting is assumed throughout the evaluation, as well as an ℓ_{∞} norm-bound threat model.

The scenarios considered – further detailed in the following – are: (a) small FCN and CNN models, adversarially trained on greyscale images; (b) RESNET, adversarially pre-trained with speed in mind on colour images; (c) RESNET, adversarially pre-trained according to *state-of-the-art* protocol on colour images.

5.1 Setup

Data In *scenario (a)*, we use the MNIST [39] and FASHIONMNIST [71] datasets; in *scenarios (b)* and *(c)*, the CIFAR-10 [35] dataset.

Architectures In *scenario (a)*, we use one fully-connected ($\approx 1.74 \times 10^5$ parameters) and one pooling-free convolutional ($\approx 1.67 \times 10^5$ parameters) three-layers networks as classifiers.

In *scenarios (b)* and *(c)*, we use as classifiers, respectively, the pre-trained RESNET-18 from [70] ($\approx 1.1 \times 10^7$ parameters) and the pre-trained RESNET-18 from [52] (1.25×10^7 parameters).

In all three cases, CARSO is composed of a one-layer convolutional input pre-encoder, FCN context pre-encoder and encoder, deep deconvolutional decoder.

Further details of architectures are given in Appendix C.

Outer minimisation In *scenario (a)*, we train (both adversarially and not) classifiers on the categorical cross-entropy loss, optimised by RADAM+LOOKAHEAD [75, 42] with *epochwise* one-cycle, cyclical learning rate [59]. In *scenarios (b)* and *(c)* classifiers are obtained as pre-trained models, from public resources made available by the respective Authors.

In all three cases, CARSO is trained on the VAE loss, using *summed pixel-wise channel-wise* binary cross entropy as reconstruction cost. Optimisation is performed by RADAM+LOOKAHEAD with *epochwise* one-cycle, cyclical learning rate.

Scenario- and *architecture-*specific details are provided in Appendix C.

Inner minimisation The $\epsilon_\infty = 0.3$ threat model is assumed for the MNIST and FASHIONMNIST datasets, whereas $\epsilon_\infty = 8/255$ is considered for CIFAR-10.

For adversarial training of classifiers in *scenario (a)*, and training of CARSO in all three cases – adversarial examples are obtained by maximising the categorical cross-entropy between the prediction made by the classifier on a clean input, and that made on the perturbed input, in a *class-untargeted* fashion.

In adversarial training within *scenario (a)*, attacks are performed against the current parameters of the model, replacing them after each parameter update step. Perturbations are obtained using mixed PGD $_{\epsilon_\infty}^{40}$ and PGD $_{\epsilon_\infty/2}^{40}$ by gradient ascent with a step size of 0.01 (given [0, 1] scaled data).

In all three *scenarios*, examples for the training of CARSO are obtained according to procedure described in subsection 4.4 – in the case of PGD, optimised by gradient ascent with a step size of 0.01.

Full details and hyperparameters of the attacks are described in Appendix C.

Evaluation In all scenarios, we report the robust test-set accuracy by means of AUTOATTACK (AA) [13] evaluation: *i.e.*, the worst-case accuracy on a mixture of AUTOPGD on the cross-entropy loss [13] with 100 steps, AUTOPGD on the *difference of logits ratio* loss [13] with 100 steps, FAB [12] with 100 steps, and the *black-box* SQUARE attack [1] with 5000 queries. Such attacks are performed against the undefended classifier, and against the undefended classifier which is then defended by CARSO with *mode* aggregation.

For evaluation of the ‘classifier+CARSO’ architecture as a whole, the version of AA suitable for stochastic defences is used (as the sampling in the generative denoising part of CARSO produces non-deterministic forward passes). The mixture of attacks is composed, in this case, of AUTOPGD on both the cross-entropy and *difference of logits ratio* losses, with 100 steps, and 20 EOT [3] iterations. The number of purified samples per input to be generated is set to 4, and aggregation approximated as per-class *sum of softmaxes* to make it exactly differentiable.

In *scenarios (a)* and *(b)*, robust accuracy is additionally evaluated with the following attacks against the classifier: DEEPFOOL $_{3\epsilon_\infty/2; \epsilon_\infty; \epsilon_\infty/2}$ [47], PGD $_{3\epsilon_\infty/2; \epsilon_\infty}^{40}$, FGSM $_{3\epsilon_\infty/2; \epsilon_\infty}$, A-PGD $_{3\epsilon_\infty/2; \epsilon_\infty; \epsilon_\infty/2}^{50}$ [13]; and additionally in *scenario (b)* with *end-to-end*: PGD $_{3\epsilon_\infty/2; \epsilon_\infty}^{40}$, FGSM $_{3\epsilon_\infty/2; \epsilon_\infty}$, A-PGD $_{3\epsilon_\infty/2; \epsilon_\infty; \epsilon_\infty/2}^{50}$.

Computational infrastructure All experiments have been performed on an *NVIDIA DGX A100* system housed at *AREA Science Park*. Available resources were: 32 cores (with $2\times$ hyperthreading) from a dual *AMD Rome 7742* processor, 128 GB of main memory, 1 *NVIDIA A100* with 40 GB of dedicated memory.

As an example of training efficiency – when using the *state-of-the-art* model of *scenario (c)* from [52] – the training of the purifier required <130 min.

5.2 Results and discussion

Results of experiments are shown in Table 1 and in Appendix D.

Table 1: Accuracy for the different models, datasets, and attack scenarios considered. RN-18: RESNET-18, Cl: clean training/accuracy; AA: *AutoAttack* [13]; AT: adversarial training as per section 4; C: CARSO; E2E: *end-to-end* AA for stochastic defences. Defence strategy on the left side of the solidus (*i.e.* defence/attack).

Scen.	Arch.	Cl/Cl	Cl/AA	AT/Cl	C+AT/Cl	AT/AA	C+AT/AA	C+AT/E2E
(a), MNIST	FCN	0.9862	0.0	0.9405	0.9435	0.3838	0.8441	
(a), MNIST	CNN	0.9927	0.0	0.9868	0.9865	0.7721	0.9298	
(a), FMNIST	CNN	0.9063	0.0	0.7825	0.7853	0.3836	0.6769	
(b), CIFAR-10	RN-18 [70]			0.8380	0.7755	0.4336	0.5571	0.7096
(c), CIFAR-10	RN-18 [52]			0.8353	0.7824	0.5668	0.6285	0.6648

Scenario (a) *Clean* accuracy for classifiers trained non-adversarially on MNIST is close to 1.0. In this setting, though, vulnerability to adversarial attacks is total and constitutes a significant threat. PGD adversarial training – even though rudimentary in protocol – is able to mitigate the issue, at a slight decrease in *clean* accuracy. However, if we move beyond the kind of attacks considered during training, or beyond the threat model by including evaluation against stronger attacks, said mitigation is unsatisfactory.

The defence provided by CARSO enhances the effects of adversarial training on robustness, sometimes even slightly reversing the *side-effects* it induces: an additional improvement in robustness is observed against *foreseen* attacks, and *clean accuracy* is preserved – or improved thanks to the denoising ability of the generative model. A significant increase in robustness is shown against *unforeseen* attacks (both in type and strength) – particularly in the case of DEEPFOOL, where the absolute increase in robust accuracy at $\epsilon_\infty = 0.3$ is ≈ 0.31 , and at $3\epsilon_\infty/2$ even ≈ 0.72 (*i.e.* a more than 10-fold relative increase). The same considerations do apply to FASHIONMNIST, with the only exception of a decrease in accuracies across all tests due to the increased complexity of the task. Full results are available in Appendix D.

Such findings corroborate the claims made in subsection 4.2 and a positive evaluation of the method.

Scenario (b) In this setting, the adversarially-trained classifier is able to provide some robustness from perturbative attacks, despite suffering the limits of a speed-focused training protocol. This is even more evident against unforeseen attacks, *i.e.* DEEPFOOL and AUTOATTACK.

Application of our defence improves robust accuracy, with a limited *clean* accuracy toll. Remarkably, the resulting architecture is able to withstand adversarial attacks to a similar extent as the adversarially-trained *state-of-the-art* model from [52] used in *scenario (c)*.

End-to-end attacks against the whole architecture appear less effective *w.r.t.* attacks towards the classifier alone defended *a posteriori*. A graphical report of results is provided by Figure 1, whereas exact results are shown in Appendix D.

Scenario (c) The RESNET-18 trained according to [52] is, to the best of our knowledge, the *state-of-the-art* model for such architecture adversarially-trained on CIFAR-10 without use of additional synthetic data. In this case, robustness against even unforeseen attacks is significant – and reached without excessive damage to *clean* accuracy.

In such scenario, still, the adoption of CARSO clearly improves robust accuracy of the model, at the cost of non-negligible – but still acceptable – decrease in *clean* accuracy. Indeed, the increase in

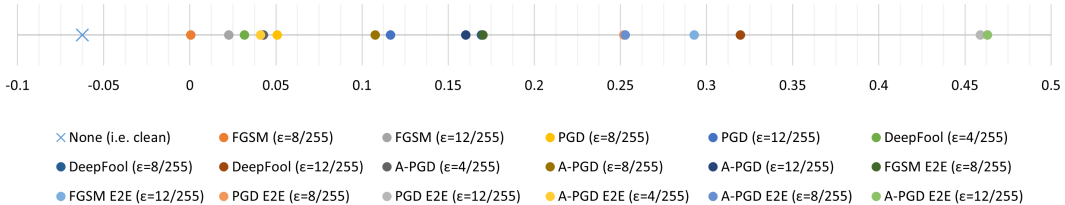


Figure 1: Variation in test set (robust) accuracy between the RESNET-18 from [70] in *scenario (b)* with and without the addition of CARSO, across different attacks. Exact results in Table 10.

robustness is, both in absolute and relative terms, advantageous *w.r.t.* the associated damage to *clean* accuracy, and the resulting model is still useful even in case a limited portion of test examples is assumed to be adversarial. As in previous scenarios, the addition of CARSO does not reduce overall robustness when *end-to-end* attacks are produced against the entire architecture.

This confirms a significantly positive evaluation of the approach *w.r.t.* existing defences based on adversarial training.

Further experimentation In order to better corroborate the conjecture introduced in subsection 4.2, an *ad hoc* experiment is performed on the architecture from *scenario (c)*. The AA routine for stochastic defences is used to directly perturb the *internal representation* extracted from the classifier, obtained from clean inputs. Results show a *close-to-zero* robust accuracy (*i.e.* 0.0406 exactly) – confirming the relevance of the interaction between *internal representation* and *model*, in the robust functioning of CARSO.

5.3 Limitations and open problems

In line with recent works aiming at robustness against multiple perturbations [17, 37], our method imposes a decrease in *clean* accuracy *w.r.t.* the adversarially-pretrained undefended counterpart. In an attempt to improve cross-talk between *classifier* and *purifier* without harming robustness – such issue may be tentatively addressed, in our case, by an approach similar to that from [41]. The effect on the resulting *end-to-end* robustness should be explicitly re-evaluated in such case.

Additionally, scalability issues may complicate the application of CARSO – as it requires the training of the purifier, whose input is linear in the number of neurons of the classifier. Using a subset of layers as a surrogate for the entire *internal representation* – as described in subsection 4.5 – does mitigate the problem in practice. This, however, comes at the cost of having to find the most suitable of such subsets – a fully handcrafted task at the moment.

6 Conclusion

In this work, we presented a novel adversarial defence mechanism tightly integrating input *purification*, and classification by an adversarially-pretrained model, – being ultimately able to improve upon *state-of-the-art* adversarial training approaches across a variety of benchmark tasks. Such results show the value of CARSO as a viable strategy to improve adversarial robustness in visual tasks, additionally offering increased computational efficiency and faster inference times *w.r.t.* novel contemporary approaches.

The promising, positive evaluation of the method within the scope investigated suggests potential future extensions beyond images as input. Additionally – though we expect similar behaviour to that already observed – we plan to further extend the experimental scope of our analysis to larger models (both in the number of parameters and *internal representation*) and different architectures (*e.g.* non-convolutional).

Such endeavour will in turn require a deeper understanding and the development of general criteria for the selection of relevant subsets of *internal representation* – to be used in the conditioning of the purification model. Candidate approaches in this regard may be rooted in the analysis of *layerwise intrinsic dimension* [2], or *ad-hoc* metrics to quantify the most informative neurons.

References

- [1] Maksym Andriushchenko et al. ‘Square Attack: a query-efficient black-box adversarial attack via random search’. In: *16th European Conference on Computer Vision*. 2020.
- [2] Alessio Ansuini et al. ‘Intrinsic dimension of data representations in deep neural networks’. In: *Advances in Neural Information Processing Systems*. 2019.
- [3] Anish Athalye et al. ‘Synthesizing Robust Adversarial Examples’. In: *Proceedings of the International Conference on Machine Learning*. 2018.
- [4] Vincent Ballet et al. ‘Imperceptible Adversarial Attacks on Tabular Data’. In: *Thirty-third Conference on Neural Information Processing Systems, Workshop on Robust AI in Financial Services: Data, Fairness, Explainability, Trustworthiness, and Privacy (Robust AI in FS)*. 2019.
- [5] Battista Biggio and Fabio Roli. ‘Wild patterns: Ten years after the rise of adversarial machine learning’. In: *Pattern Recognition* 84 (2018), pp. 317–331.
- [6] Battista Biggio et al. ‘Evasion Attacks against Machine Learning at Test Time’. In: *Proceedings of the 2013th European Conference on Machine Learning and Knowledge Discovery in Databases - Volume Part III*. 2013.
- [7] Luca Bortolussi and Guido Sanguinetti. *Intrinsic Geometric Vulnerability of High-Dimensional Artificial Intelligence*. 2018. arXiv: 1811.03571.
- [8] Léon Bottou. ‘On-Line Algorithms and Stochastic Approximations’. In: *On-Line Learning in Neural Networks*. Ed. by David Saad. Cambridge University Press, 1999.
- [9] Ginevra Carbone et al. ‘Robustness of Bayesian Neural Networks to Gradient-Based Attacks’. In: *Advances in Neural Information Processing Systems*. 2020.
- [10] Nicholas Carlini et al. *On Evaluating Adversarial Robustness*. 2019. arXiv: 1902.06705.
- [11] Moustapha Cisse et al. ‘Parseval Networks: Improving Robustness to Adversarial Examples’. In: *Proceedings of the International Conference on Machine Learning*. 2017.
- [12] Francesco Croce and Matthias Hein. *Minimally distorted Adversarial Examples with a Fast Adaptive Boundary Attack*. 2020. arXiv: 1907.02044.
- [13] Francesco Croce and Matthias Hein. ‘Reliable Evaluation of Adversarial Robustness with an Ensemble of Diverse Parameter-free Attacks’. In: *Proceedings of the International Conference on Machine Learning*. 2020.
- [14] Francesco Croce et al. ‘RobustBench: a standardized adversarial robustness benchmark’. In: *Thirty-fifth Conference on Neural Information Processing Systems Datasets and Benchmarks Track (Round 2)*. 2021.
- [15] Jia Deng et al. ‘ImageNet: A large-scale hierarchical image database’. In: *IEEE Conference on Computer Vision and Pattern Recognition*. 2009.
- [16] Gavin Weiguang Ding, Luyu Wang and Xiaomeng Jin. *AdverTorch v0.1: An Adversarial Robustness Toolbox based on PyTorch*. 2019. arXiv: 1902.07623.
- [17] Hadi M. Dolatabadi, Sarah Erfani and Christopher Leckie. ‘ ℓ_∞ -Robustness and Beyond: Unleashing Efficient Adversarial Training’. In: *18th European Conference on Computer Vision*. 2022.
- [18] James Eric Eich. ‘The cue-dependent nature of state-dependent retrieval’. In: *Memory & Cognition*. 1980.
- [19] Ian Goodfellow, Jonathon Shlens and Christian Szegedy. ‘Explaining and Harnessing Adversarial Examples’. In: *International Conference on Learning Representations*. 2015.
- [20] Ian Goodfellow et al. ‘Generative Adversarial Nets’. In: *Advances in Neural Information Processing Systems*. 2014.
- [21] Sven Gowal et al. ‘Improving Robustness using Generated Data’. In: *Advances in Neural Information Processing Systems*. 2021.
- [22] Sven Gowal et al. *Uncovering the Limits of Adversarial Training against Norm-Bounded Adversarial Examples*. 2020. arXiv: 2010.03593.
- [23] Shixiang Gu and Luca Rigazio. ‘Towards Deep Neural Network Architectures Robust to Adversarial Examples’. In: *Workshop Track of the International Conference on Learning Representations*. 2015.
- [24] Kaiming He et al. ‘Deep Residual Learning for Image Recognition’. In: *IEEE Conference on Computer Vision and Pattern Recognition*. 2016.
- [25] Mitch Hill, Jonathan Mitchell and Song-Chun Zhu. ‘Stochastic Security: Adversarial Defense Using Long-Run Dynamics of Energy-Based Models’. In: *International Conference on Learning Representations*. 2021.
- [26] Chin-Wei Huang, Jae Hyun Lim and Aaron C Courville. ‘A Variational Perspective on Diffusion-Based Generative Models and Score Matching’. In: *Advances in Neural Information Processing Systems*. 2021.
- [27] Matthew Hutson. ‘Eye-catching advances in some AI fields are not real’. In: *Science*. 2020.
- [28] Uiwon Hwang et al. ‘PuVAE: A Variational Autoencoder to Purify Adversarial Examples’. In: *IEEE Access*. 2019.

- [29] Andrew Ilyas et al. ‘Adversarial Examples Are Not Bugs, They Are Features’. In: *Advances in Neural Information Processing Systems*. 2019.
- [30] Alessandro Ingrosso and Sebastian Goldt. ‘Data-driven emergence of convolutional structure in neural networks’. In: *Proceedings of the National Academy of Sciences* 119.40 (2022), e2201854119.
- [31] Pavel Izmailov et al. ‘Averaging weights leads to wider optima and better generalization’. In: *Conference on Uncertainty in Artificial Intelligence*. 2018.
- [32] Xiaojun Jia et al. ‘LAS-AT: Adversarial Training With Learnable Attack Strategy’. In: *Proceedings of the IEEE/CVF Conference on Computer Vision and Pattern Recognition*. 2022.
- [33] Hoki Kim. *Torchattacks: A PyTorch repository for adversarial attacks*. 2020. arXiv: 2010.01950.
- [34] Diederik P. Kingma and Max Welling. ‘Auto-Encoding Variational Bayes’. In: *International Conference on Learning Representations*. 2014.
- [35] Alex Krizhevsky. ‘Learning Multiple Layers of Features from Tiny Images’. In: 2009.
- [36] Alexey Kurakin, Ian J. Goodfellow and Samy Bengio. ‘Adversarial Examples in the Physical World’. In: *Artificial Intelligence Safety and Security* (2018).
- [37] Cassidy Laidlaw, Sahil Singla and Soheil Feizi. ‘Perceptual Adversarial Robustness: Defense Against Unseen Threat Models’. In: *International Conference on Learning Representations*. 2021.
- [38] Y. LeCun et al. ‘Gradient-based learning applied to document recognition’. In: *Proceedings of the IEEE* 86.11 (1998), pp. 2278–2324.
- [39] Yann LeCun and Corinna Cortes. *The MNIST handwritten digit database*. 2010.
- [40] Yann LeCun et al. ‘A tutorial on energy-based learning’. In: *Predicting structured data*. Ed. by G. Bakir et al. MIT Press, 2006.
- [41] Fangzhou Liao et al. ‘Defense Against Adversarial Attacks Using High-Level Representation Guided Denoiser’. In: *IEEE Conference on Computer Vision and Pattern Recognition*. 2018.
- [42] Liyuan Liu et al. ‘On the Variance of the Adaptive Learning Rate and Beyond’. In: *International Conference on Learning Representations*. 2020.
- [43] Aleksander Madry et al. ‘Towards Deep Learning Models Resistant to Adversarial Attacks’. In: *International Conference on Learning Representations*. 2018.
- [44] J.J. Medina. ‘The Biology of Recognition Memory’. In: *Psychiatric Times*. 2008.
- [45] Diganta Misra. ‘Mish: A self regularized non-monotonic neural activation function’. In: *Proceedings of the British Machine Vision Conference*. 2020.
- [46] Tom M. Mitchell. *The Need for Biases in Learning Generalizations*. Tech. rep. New Brunswick, NJ: Rutgers University, 1980.
- [47] Seyed-Mohsen Moosavi-Dezfooli, Alhussein Fawzi and Pascal Frossard. ‘DeepFool: A Simple and Accurate Method to Fool Deep Neural Networks’. In: *IEEE Conference on Computer Vision and Pattern Recognition*. 2016.
- [48] Weili Nie et al. ‘Diffusion Models for Adversarial Purification’. In: *Proceedings of the International Conference on Machine Learning*. 2022.
- [49] Adam Paszke et al. ‘PyTorch: An Imperative Style, High-Performance Deep Learning Library’. In: *Advances in Neural Information Processing Systems*. 2019.
- [50] Yunchen Pu et al. ‘Variational Autoencoder for Deep Learning of Images, Labels and Captions’. In: *Advances in Neural Information Processing Systems*. 2016.
- [51] Yao Qin et al. ‘Imperceptible, Robust, and Targeted Adversarial Examples for Automatic Speech Recognition’. In: *Proceedings of the International Conference on Machine Learning*. 2019.
- [52] Sylvestre-Alvise Rebuffi et al. ‘Data Augmentation Can Improve Robustness’. In: *Advances in Neural Information Processing Systems*. 2021.
- [53] Danilo Jimenez Rezende, Shakir Mohamed and Daan Wierstra. ‘Stochastic Backpropagation and Approximate Inference in Deep Generative Models’. In: *Proceedings of the International Conference on Machine Learning*. 2014.
- [54] Leslie Rice, Eric Wong and J. Zico Kolter. ‘Overfitting in adversarially robust deep learning’. In: *Proceedings of the International Conference on Machine Learning*. 2020.
- [55] Herbert Robbins and Sutton Monro. ‘A Stochastic Approximation Method’. In: *The Annals of Mathematical Statistics* 22.3 (1951), pp. 400–407.
- [56] Pouya Samangouei, Maya Kabkab and Rama Chellappa. ‘Defense-GAN: Protecting Classifiers Against Adversarial Attacks Using Generative Models’. In: *International Conference on Learning Representations*. 2018.
- [57] Changhao Shi, Chester Holtz and Gal Mishne. ‘Online Adversarial Purification based on Self-supervised Learning’. In: *International Conference on Learning Representations*. 2021.
- [58] Naman D Singh, Francesco Croce and Matthias Hein. *Revisiting Adversarial Training for ImageNet: Architectures, Training and Generalization across Threat Models*. 2023. arXiv: 2303.01870.

- [59] Leslie N. Smith. ‘Cyclical Learning Rates for Training Neural Networks’. In: *IEEE Winter Conference on Applications of Computer Vision*. 2017.
- [60] Kihyuk Sohn, Honglak Lee and Xinchen Yan. ‘Learning Structured Output Representation using Deep Conditional Generative Models’. In: *Advances in Neural Information Processing Systems*. 2015.
- [61] Christian Szegedy et al. ‘Intriguing properties of neural networks’. In: *International Conference on Learning Representations*. 2014.
- [62] Florian Tramèr. ‘Detecting Adversarial Examples Is (Nearly) As Hard As Classifying Them’. In: *Proceedings of the International Conference on Machine Learning*. 2022.
- [63] Florian Tramèr and Dan Boneh. ‘Adversarial Training and Robustness for Multiple Perturbations’. In: *Advances in Neural Information Processing Systems*. 2019.
- [64] Florian Tramèr et al. ‘Ensemble Adversarial Training: Attacks and Defenses’. In: *International Conference on Learning Representations*. 2018.
- [65] Florian Tramèr et al. ‘On Adaptive Attacks to Adversarial Example Defenses’. In: *Advances in Neural Information Processing Systems*. 2020.
- [66] Endel Tulving and Donald M. Thomson. ‘Encoding specificity and retrieval processes in episodic memory’. In: *Psychological Review*. 1973.
- [67] Jonathan Uesato et al. ‘Adversarial Risk and the Dangers of Evaluating Against Weak Attacks’. In: *Proceedings of the International Conference on Machine Learning*. 2018.
- [68] Pascal Vincent et al. ‘Extracting and composing robust features with denoising autoencoders’. In: *International Conference on Machine Learning*. 2008.
- [69] Zekai Wang et al. *Better Diffusion Models Further Improve Adversarial Training*. 2023. arXiv: 2303.10130.
- [70] Eric Wong, Leslie Rice and J. Zico Kolter. ‘Fast is better than free: Revisiting adversarial training’. In: *International Conference on Learning Representations*. 2020.
- [71] Han Xiao, Kashif Rasul and Roland Vollgraf. *Fashion-MNIST: a Novel Image Dataset for Benchmarking Machine Learning Algorithms*. 2017. arXiv: 1708.07747.
- [72] Xinchen Yan et al. ‘Attribute2Image: Conditional Image Generation from Visual Attributes’. In: *Proceedings of the European Conference on Computer Vision*. 2016.
- [73] Jongmin Yoon, Sung Ju Hwang and Juho Lee. ‘Adversarial Purification with Score-based Generative Models’. In: *Proceedings of the International Conference on Machine Learning*. 2021.
- [74] M. Zhang, S. Levine and C. Finn. ‘MEMO: Test Time Robustness via Adaptation and Augmentation’. In: *Advances in Neural Information Processing Systems*. 2022.
- [75] Michael Zhang et al. ‘Lookahead Optimizer: k steps forward, 1 step back’. In: *Advances in Neural Information Processing Systems*. 2019.
- [76] Zhaoyu Zhang, Mengyan Li and Jun Yu. ‘On the Convergence and Mode Collapse of GAN’. In: *SIG-GRAPH Asia 2018 Technical Briefs*. 2018.

A On the functioning of (conditional) Variational Autoencoders

Variational autoencoders (VAEs) [34, 53] learn from data a generative distribution of the form $p(\mathbf{x}, \mathbf{z}) = p(\mathbf{x} | \mathbf{z})p(\mathbf{z})$, where probability density $p(\mathbf{z})$ represents a prior over latent variable \mathbf{z} , and $p(\mathbf{x} | \mathbf{z})$ is the likelihood function, which can be used to sample data of interest \mathbf{x} , given \mathbf{z} .

Training is carried out by maximising a variational lower bound $-\mathcal{L}_{\text{VAE}}(\mathbf{x})$ on the log-likelihood $\log p(\mathbf{x})$ – which is a proxy for the *Evidence Lower Bound (ELBO)* – i.e.:

$$-\mathcal{L}_{\text{VAE}}(\mathbf{x}) := \mathbb{E}_{q(\mathbf{z} | \mathbf{x})}[\log p(\mathbf{x} | \mathbf{z})] - \text{KL}(q(\mathbf{z} | \mathbf{x}) \| p(\mathbf{z}))$$

where $q(\mathbf{z} | \mathbf{x}) \approx p(\mathbf{z} | \mathbf{x})$ is an approximate posterior and $\text{KL}(\cdot \| \cdot)$ is the Kullback-Leibler divergence.

By parameterising likelihood with a *decoder ANN* $p_{\theta_D}(\mathbf{x} | \mathbf{z}; \theta_D) \approx p(\mathbf{x} | \mathbf{z})$, and a possible variational posterior with an *encoder ANN* $q_{\theta_E}(\mathbf{z} | \mathbf{x}; \theta_E) \approx q(\mathbf{z} | \mathbf{x})$, the parameters θ_D^* of the generative model better reproducing the data may be learned – jointly with θ_E^* as:

$$\begin{aligned} \theta_E^*, \theta_D^* &:= \\ &\arg \min_{(\theta_E, \theta_D)} \mathcal{L}_{\text{VAE}}(\mathbf{x}) = \\ &\arg \min_{(\theta_E, \theta_D)} \mathbb{E}_{\mathbf{x} \sim \mathcal{D}} \left[-\mathbb{E}_{\mathbf{z} \sim q_{\theta_E}(\mathbf{z} | \mathbf{x}; \theta_E)} [\log p_{\theta_D}(\mathbf{x} | \mathbf{z}; \theta_D)] + \text{KL}(q_{\theta_E}(\mathbf{z} | \mathbf{x}; \theta_E) \| p(\mathbf{z})) \right] \end{aligned}$$

where \mathcal{D} is the distribution over (training) examples \mathbf{x} .

From the practical viewpoint, optimisation relies on the empirical evaluation of $\mathcal{L}_{\text{VAE}}(\mathbf{x}; \theta)$ on minibatches of data, with $-\mathbb{E}_{\mathbf{z} \sim q_{\theta_E}(\mathbf{z} | \mathbf{x}; \theta_E)} [\log p_{\theta_D}(\mathbf{x} | \mathbf{z}; \theta_D)]$ replaced by a *reconstruction cost*

$$\mathcal{L}_{\text{Reco}}(\mathbf{x}, \mathbf{x}') \geq 0 \mid \mathcal{L}_{\text{Reco}}(\mathbf{x}, \mathbf{x}') = 0 \iff \mathbf{x} = \mathbf{x}' .$$

Generation of new data according to the fitted model is achieved by sampling from

$$p_{\theta_D^*}(\mathbf{x} | \mathbf{z}; \theta_D^*) \Big|_{\mathbf{z} \sim p(\mathbf{z})}$$

i.e. decoding samples from $p(\mathbf{z})$.

The setting is analogous in the case of *conditional* Variational Autoencoders [60, 72] (see section 3), where (conditional) sampling is achieved by

$$\mathbf{x}_{c_j} \sim p_{\theta_D^*}(\mathbf{x} | \mathbf{z}, \mathbf{c}; \theta_D^*) \Big|_{\mathbf{z} \sim p(\mathbf{z}); \mathbf{c} = \mathbf{c}_j} .$$

B Justification of Adversarially-balanced batches

During the incipient phases of experimentation, the following *phenomena* were observed in *scenario (a)*-like settings. The classifier was kept frozen, shielded with CARSO, and attacked adversarially.

If the purification machinery had been trained with PGD-generated adversarial examples only – the standard *de facto* for adversarial training of classifiers:

- (a) Unsatisfactory *clean* accuracy was reached upon convergence, speculatively as a consequence of the VAE never having been trained on *clean-to-clean* example *denoising*;
- (b) Persistent vulnerability to same norm-bound FGSM perturbations was noticed, sometimes even higher *w.r.t.* the undefended model;
- (c) Persistent vulnerability to smaller norm-bound FGSM and PGD perturbation was noticed, a phenomenon usually absent in the undefended model.

In order to tentatively mitigate such issues, the composition of adversarial examples was adapted to specifically counter each of the pitfalls identified. Adoption of any subset smaller than that described in subsection 4.4 resulted in unsatisfactory accuracy *w.r.t.* one of the (sub)cases listed above.

At that point, another problem emerged: if the *adapted* adversarial training protocol had been carried out by showing the *purifier* homogeneous batches of adversarially-perturbed (or clean) examples, the resulting test accuracy across the *problematic* sub-cases listed above was higher for recently-seen batches, and decreasing otherwise.

Such observation lead to the final formulation of the training protocol (see subsection 4.4), which mitigates successfully all the issues described.

C Architectural details and hyperparameters

In the section that follows, we provide exact details about the architectures (subsection C.1) and hyperparameters (subsection C.2) used in the experimental phase of our work. Data are reported mostly in the form of tables, with explanatory captions and eventual additional explanatory text.

C.1 Architectures

In this section, we describe the architectural choices for non-*pretrained* models, including individual parts of the CARSO purifier. Architectures used for the *FCN* and *CNN* classifier models in *scenario (a)* are provided in Table 2. In the case of RESNET models (*scenarios (b)* and *(c)*), the pre-trained PREACTRESNET-18 from [70] and RESNET-18 from [52] are used. Regardless of the original implementation choices, an initial normalisation layer is always included as part of the model (and as such, attackable by adversaries). In the case of CIFAR-10 such layer is applied channel-wise, *i.e.* it is so defined: $\text{Normalisation}(\mu = (0.4914, 0.4822, 0.4465), \sigma = (0.2471, 0.2435, 0.2616))$.

Table 2: Architectures for the *FCN* and *CNN* models used in *scenario (a)* for the MNIST dataset. In the description of convolutional layers, the following shorthand notation is used: *ch_in*: number of input channels, *ch_out*: number of output channels, *k*: square kernel size, *s*: isotropic stride, *p*: isotropic padding. Convolutional layers are to be intended *bias-free* if a Batch Normalisation layer follows, *biased* otherwise. The *CNN* model used for the FASHIONMNIST dataset is identical to the one used for MNIST (shown below), but does not include the initial data-normalisation layer.

<i>FCN</i>	<i>CNN</i>
Normalisation($\mu = 0.1307$; $\sigma = 0.3081$)	Normalisation($\mu = 0.1307$; $\sigma = 0.3081$)
Linear(features_in=786, features_out=200)	Conv2D(ch_in=1, ch_out=16, k=4, s=2, p=1)
Batch Normalisation	Mish [45]
Mish	Batch Normalisation
Dropout(p=0.15)	Conv2D(ch_in=16, ch_out=32, k=4, s=2, p=1)
Linear(features_in=200, features_out=80)	Mish
Batch Normalisation	Batch Normalisation
Mish	Flatten
Dropout(p=0.15)	Dropout(p=0.1)
Linear(features_in=80, features_out=10)	Linear(features_in=1568, features_out=100)
Mish	Mish
Softmax	Batch Normalisation
	Dropout(p=0.1)
	Linear(features_in=80, features_out=10)
	Softmax

The *input pre-encoder* used as part of CARSO is always composed of one *biased* convolutional layer with kernel size= 4, stride= 1 and padding= 0. The number of input channels is the same as the input (*i.e.* 1 for MNIST and FASHIONMNIST data; 3 for CIFAR-10 data). The number of output channels is the least – compatible with given *kernel size*, *stride*, and *padding* – such that the number of scalars necessary to represent the *pre-encoded input* is greater or equal to that of *input* itself. *Implementation-wise*, such number is computed programmatically and never set explicitly. This choice never results in an actual input *compression*.

Architectures used for the *representation pre-encoder* and *actual* encoder of CARSO are shown in Table 3. The exact (eventual subset of) layers used as *internal representation* on a case-by-case basis are reported in subsection C.2, additional hyperparameters left unspecified in Table 3 are provided in Table 6.

Table 3: Architectures for *representation pre-encoder* and *actual* encoder of CARSO. Symbols f_i and f_o denote respectively the number of input features in and output features of the given encoder. Specific values for different scenarios, datasets, and architectures are reported in Table 6.

<i>Repr. pre-encoder</i>	Encoder
Linear(features_in= f_i , features_out= $2 \times f_o$)	Linear(features_in= f_i , features_out= $f_i + f_o/2$)
Batch Normalisation	Batch Normalisation
LeakyReLU(slope=0.01)	LeakyReLU(slope=0.01)
Linear(features_in= $2 \times f_o$, features_out= f_o)	Dropout(p=0.0375)
Batch Normalisation	Linear(features_in= $f_i + f_o/2$, features_out= f_o)
LeakyReLU(slope=0.01)	Batch Normalisation
Sigmoid	LeakyReLU(slope=0.01)
	Tanh

The sampler used within CARSO for generation of latent variable z during training is a reparameterised [34] Normal sampler $z \sim \mathcal{N}(\mu_e, \sigma_e)$ whose characteristic parameters μ_e and σ_e are the output of two independent Linear layers receiving as input the same output of the *actual* encoder. The output size of the sampler is provided in Table 6. The sampler used within CARSO for generation of latent variable z during inference (*i.e.* its *prior*) is a reparameterised *i.i.d* Standard Normal sampler $z \sim \mathcal{N}(0, 1)$.

Architectures used as *decoder* within CARSO are shown in Table 4, according to the specific data to be generated. The number of output channels c_o are the same as the original data whose denoising is performed (*i.e.* 1 for MNIST and FASHIONMNIST data; 3 for CIFAR-10 data). The number of input channels c_i is the Sample Size provided in Table 6.

Table 4: Architectures for the CARSO decoder, according to the type of *purified* data to be generated. Entries listed under the -NIST title refer to MNIST and FASHIONMNIST data. The name TrConv denotes transposed convolutions. In the description of deconvolutional layers, the following shorthand notation is used: ch_in: number of input channels, ch_out: number of output channels, k: square kernel size, s: isotropic stride, p: isotropic padding. Deconvolutional layers are to be intended *bias-free* if a Batch Normalisation layer follows, *biased* otherwise. Symbols c_i and c_o denote respectively the number of input channels in and output channels of the given decoder.

-NIST	CIFAR-10
TrConv2D(ch_in= c_i , ch_out= $c_i/2$, k=4, s=1, p=0)	TrConv2D(ch_in= c_i , ch_out= $c_i/2$, k=4, s=1, p=0)
LeakyReLU(slope=0.01)	Batch Normalisation
TrConv2D(ch_in= $c_i/2$, ch_out= $c_i/4$, k=4, s=2, p=1)	LeakyReLU(slope=0.01)
LeakyReLU(slope=0.01)	TrConv2D(ch_in= $c_i/2$, ch_out= $c_i/4$, k=4, s=2, p=1)
TrConv2D(ch_in= $c_i/4$, ch_out= $c_i/8$, k=4, s=2, p=2)	Batch Normalisation
LeakyReLU(slope=0.01)	LeakyReLU(slope=0.01)
TrConv2D(ch_in= $c_i/8$, ch_out= c_o , k=4, s=2, p=1)	TrConv2D(ch_in= $c_i/4$, ch_out= $c_i/8$, k=4, s=2, p=1)
Sigmoid	Batch Normalisation
	LeakyReLU(slope=0.01)
	TrConv2D(ch_in= $c_i/8$, ch_out= c_o , k=4, s=2, p=1)
	Batch Normalisation
	Sigmoid

C.2 Hyperparameters

In this subsection, we describe the hyperparameters for adversarial example generation (used both during *adversarial training* and *evaluation*), model architectures, and training.

Attacks Hyperparameters for the specific adversarial attacks employed are shown in Table 5. The value of ϵ_∞ is chosen according to the specific scenario and use of the attack. With the only exception of ϵ_∞ , AUTOATTACK is to be considered *hyperparameter-free*.

Table 5: Hyperparameters for the non-*parameter-free* attacks (*i.e.* with the exception of AUTOATTACK) used in the experimental phase of this work. The entry ϵ_∞ denotes the ℓ_∞ bound of the attack, CCE denotes the *Categorical CrossEntropy* loss function, N. A. indicates a non-applicable field for the specific attack. The ℓ_∞ threat model is assumed, and all inputs are linearly rescaled within $[0.0, 1.0]$ before the attack.

	FGSM	PGD	A-PGD	DEEPFOOL
Input clipping	[0.0, 1.0]	[0.0, 1.0]	[0.0, 1.0]	[0.0, 1.0]
# of steps	1	40	50	50
Step size	ϵ_∞	0.01	0.05	0.1
Loss function	CCE	CCE	CCE	CCE
Optimiser	N.A.	SGD	SGD	N.A.
Overshoot	N.A.	N.A.	N.A.	0.02

Architectures From both the FCN and CNN architectures used in *scenario (a)*, the entire *internal representation* is given to the *representation pre-encoder* as input. As far as the RESNETS from *scenarios (a)* and *(b)* are concerned, the subset of layers provided in Table 7 is used. Names of the layers refer to that used in the corresponding implementation.

Table 6: Architectural hyperparameters for the *representation pre-encoder* and *actual encoder* used within CARSO. Output size for the z sampler is also reported. *Implementation-wise*, input sizes for the encoder are never set explicitly, but computed from the concatenation of *pre-encoded representation* and *pre-encoded input*.

	Repr. pre-enc. f_i	Repr. pre-enc. f_o	Enc. f_i	Enc. f_o	Sample size
FCN	290	130	(computed)	96	64
CNN	4814	130	(computed)	96	64
RESNET-18 [70, 52]	2.04810×10^5	512	(computed)	192	128

Table 7: Layer names from model implementations in *scenarios (b)* and *(c)* to be used as a subset of the *internal representation* fed to the *representation pre-encoder* of CARSO. The names, though different, encode the same layers along the (essentially) same architecture.

PREACTRESNET-18 from [70]	RESNET-18 from [52]
model.layer1.1.conv2	layer_0.1.conv_2d_2
model.layer2.0.conv2	layer_1.0.conv_2d_2
model.layer2.0.shortcut.0	layer_1.0.shortcut
model.layer3.0.conv2	layer_2.0.conv_2d_2
model.layer3.0.shortcut.0	layer_2.0.shortcut
model.layer3.1.conv2	layer_2.1.conv_2d_2
model.layer4.0.conv2	layer_3.0.conv_2d_2
model.layer4.0.shortcut.0	layer_3.0.shortcut
model.layer4.1.conv2	layer_3.1.conv_2d_2
model.linear	logits

Training Hyperparameters referring to the training of *base models* (*i.e.* the FCN and CNN architectures in *scenario (a)*) and CARSO (all *scenarios*) are provided in Table 8.

Table 8: Hyperparameters for the training of non-*pretrained* models used in the experimental phase of this work. Entries listed under the *Base models* title refer to the *FCN* and *CNN* models used in *scenario (a)*, both when trained *cleanly* and *adversarially*. Entries listed under the *CARSO add-on* title refer to the training of the *CARSO* purifier alone, with the defended model frozen. The entry *CCE* denotes the *Categorical CrossEntropy* loss function, *N.A.* indicates a non-applicable field for the specific set of models. The specification of (...) within braces refers to the specific scenario(s) the entry applies to. The *epochwise* specification of the *LR* scheduler refers to the fact it is applied after each epoch (as opposed to *batchwise*, as more common in practice).

	All models	Base models	CARSO add-on
Optimiser	RADAM+LOOKAHEAD		
RADAM β_1	0.9		
RADAM β_2	0.999		
RADAM ϵ	10^{-8}		
RADAM <i>Weight Decay</i>	None		
LOOKAHEAD steps	5		
LOOKAHEAD <i>averaging decay</i>	0.8		
Loss function	CCE		
LR Scheduling	cyclical, 1 cycle, <i>epochwise</i>		
Epochs	50	50	150
Increasing LR epochs	20	50	50
Decreasing LR epochs	30	100	100
Minimum LR	10^{-8}	5×10^{-8}	5×10^{-8}
Maximum LR	5×10^{-3}	0.04608 ((a)); 0.05376 ((b), (c))	0.04608 ((a)); 0.05376 ((b), (c))
Batch size	256	256	1536
Adversarial <i>batch fraction</i>	1.0 (PGD)	1.0 (PGD)	0.4 (see subsection 4.4)
Sampled reconstructions per input	N.A.	N.A.	4

D Further experimental results

Detailed results of the additional experiments described in conclusion of subsection 5.1 are reported below. Table 9 refers to models in *scenario (a)*, whereas Table 10 refers to the model in *scenario (b)*. Figure 2, Figure 3 and Figure 4 show the increases/decreases in test set (robust) accuracy for the models in *scenario (a)*. The equivalent visualisation for *scenario (b)* is shown in Figure 1.

Table 9: Test set (robust) accuracy for additional models, datasets, and attacks, in *scenario (a)*. Accuracy with the addition of *CARSO* is reported within square brackets; the greater of the pair is **emboldened**.

	MNIST: <i>FCN</i> [+ C]	MNIST: <i>CNN</i> [+ C]	FMNIST: <i>CNN</i> [+ C]
Clean (<i>i.e.</i> no attack)	0.9405 [0.9435]	0.9868 [0.9865]	0.7825 [0.7853]
FGSM ($\epsilon_\infty = 0.30$)	0.7104 [0.8625]	0.9304 [0.9661]	0.5697 [0.7484]
FGSM ($\epsilon_\infty = 0.45$)	0.1337 [0.2671]	0.4961 [0.9084]	0.1001 [0.5068]
PGD ⁴⁰ ($\epsilon_\infty = 0.30$)	0.6203 [0.8448]	0.9005 [0.9607]	0.5628 [0.7510]
PGD ⁴⁰ ($\epsilon_\infty = 0.45$)	0.0951 [0.4120]	0.0174 [0.7657]	0.0423 [0.6043]
DEEPFOOL ($\epsilon_\infty = 0.15$)	0.8421 [0.9351]	0.9595 [0.9825]	0.6420 [0.7755]
DEEPFOOL ($\epsilon_\infty = 0.30$)	0.6166 [0.9307]	0.8709 [0.9799]	0.4698 [0.7699]
DEEPFOOL ($\epsilon_\infty = 0.45$)	0.0601 [0.7834]	0.0010 [0.9204]	0.0098 [0.5947]
A-PGD ⁵⁰ ($\epsilon_\infty = 0.15$)	0.8213 [0.9100]	0.9590 [0.9769]	0.6498 [0.7564]
A-PGD ⁵⁰ ($\epsilon_\infty = 0.30$)	0.4886 [0.8456]	0.8253 [0.9355]	0.4438 [0.6983]
A-PGD ⁵⁰ ($\epsilon_\infty = 0.45$)	0.0007 [0.0903]	0.0000 [0.1881]	0.0014 [0.1590]

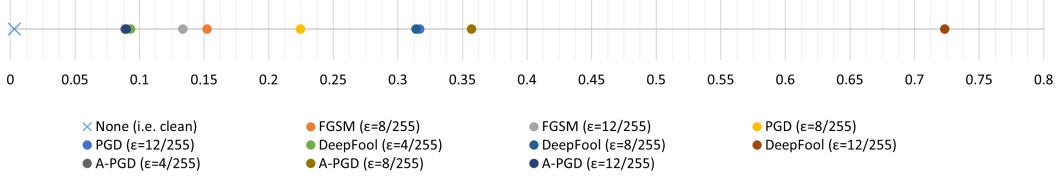


Figure 2: Variation in test set (robust) accuracy between the *FCN* from *scenario (a)* trained on MNIST, with and without the addition of CARSO, across different attacks.

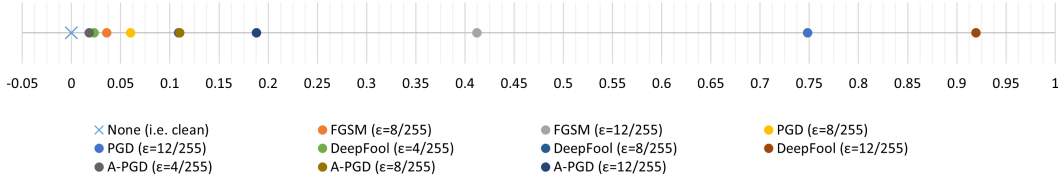


Figure 3: Variation in test set (robust) accuracy between the *CNN* from *scenario (a)* trained on MNIST, with and without the addition of CARSO, across different attacks.

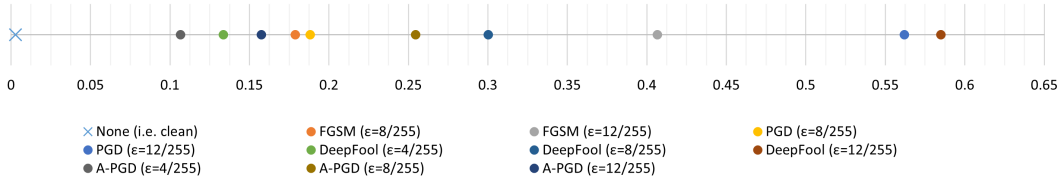


Figure 4: Variation in test set (robust) accuracy between the *CNN* from *scenario (a)* trained on FASHIONMNIST, with and without the addition of CARSO, across different attacks.

Table 10: Test set (robust) accuracy for the RESNET-18 from [70], across different attacks, in *scenario (b)*. Accuracy with the addition of CARSO is reported within square brackets; the greater of the pair is **emphasized**.

CIFAR-10: RESNET-18 [70] [+ C]	
Clean (<i>i.e.</i> no attack)	0.8380 [0.7755]
FGSM ($\epsilon_\infty = 0.30$)	0.5474 [0.5479]
FGSM ($\epsilon_\infty = 0.45$)	0.4246 [0.4471]
PGD ⁴⁰ ($\epsilon_\infty = 0.30$)	0.4657 [0.5164]
PGD ⁴⁰ ($\epsilon_\infty = 0.45$)	0.2562 [0.3726]
DEEPFOOL ($\epsilon_\infty = 0.15$)	0.6594 [0.6910]
DEEPFOOL ($\epsilon_\infty = 0.30$)	0.4491 [0.6184]
DEEPFOOL ($\epsilon_\infty = 0.45$)	0.2543 [0.5739]
A-PGD ⁵⁰ ($\epsilon_\infty = 0.15$)	0.6753 [0.7180]
A-PGD ⁵⁰ ($\epsilon_\infty = 0.30$)	0.4614 [0.5691]
A-PGD ⁵⁰ ($\epsilon_\infty = 0.45$)	0.2491 [0.4093]
FGSM ⁵⁰ E2E ($\epsilon_\infty = 0.30$)	0.5474 [0.7175]
FGSM ⁵⁰ E2E ($\epsilon_\infty = 0.45$)	0.4246 [0.7174]
PGD ⁵⁰ E2E ($\epsilon_\infty = 0.30$)	0.4657 [0.7177]
PGD ⁵⁰ E2E ($\epsilon_\infty = 0.45$)	0.2562 [0.7152]
A-PGD ⁵⁰ E2E ($\epsilon_\infty = 0.15$)	0.6753 [0.7164]
A-PGD ⁵⁰ E2E ($\epsilon_\infty = 0.30$)	0.4614 [0.7142]
A-PGD ⁵⁰ E2E ($\epsilon_\infty = 0.45$)	0.2491 [0.7122]

E Visual schematic of the CARSO architecture

A pictographic representation of the CARSO architecture is shown in Figure 5. Details are described in section 4.

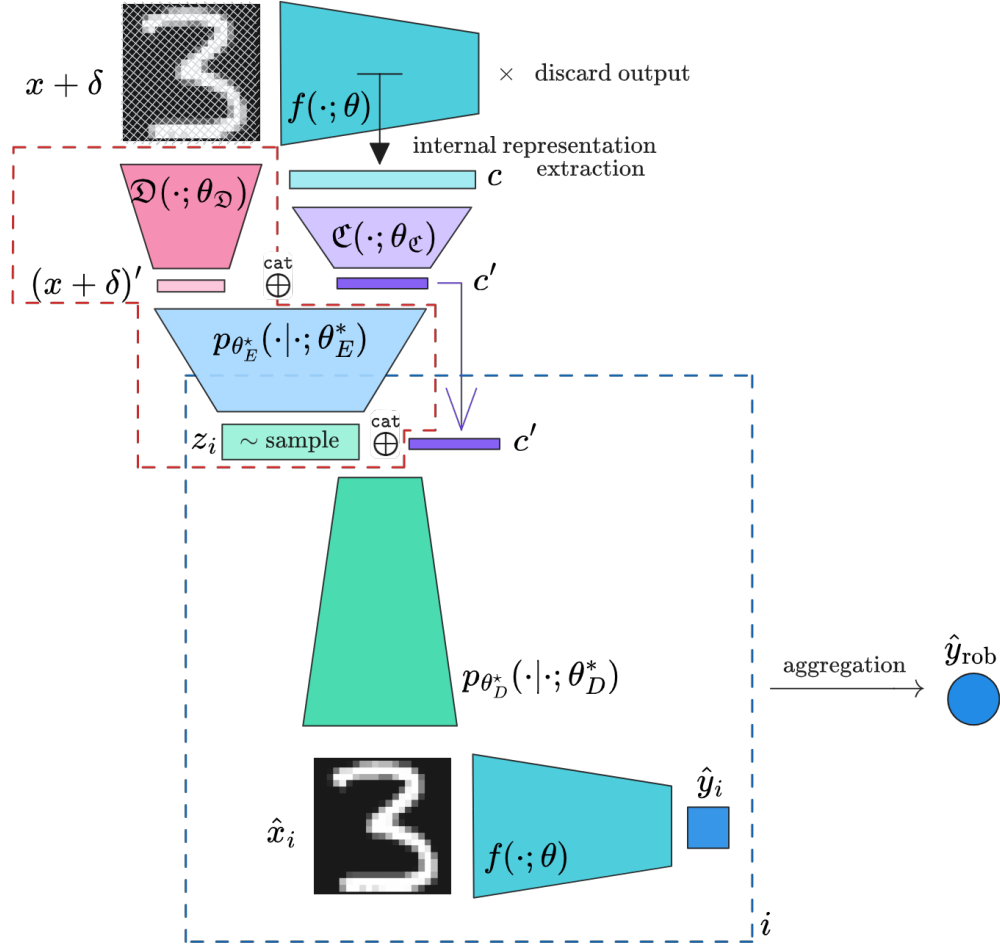


Figure 5: Schematic representation of the general architecture of CARSO. The subnetwork bordered by the red dashed line is used only during training. The subnetwork bordered by the dark blue dashed line is re-evaluated on different samples of z and the resulting individual \hat{y}_i aggregated into \hat{y}_{rob} . $f(\cdot; \theta)$ is always kept frozen; the remaining network is trained on $\mathcal{L}_{\text{VAE}}(x, \hat{x})$. During training, different δ are generated according to subsection 4.4. Precise details on the functioning of the architecture are provided in section 4.